894. Analytical modeling of Lamb wave propagation in composite laminate bonded with piezoelectric actuator based on Mindlin plate theory

Xiaoyue Zhang[1], Shenfang Yuan[2], Menglong Liu[3], Weibo Yang[4]
The State Key Laboratory of Mechanics and Control of Mechanical Structures
Nanjing University of Aeronautics and Astronautics, No. 29 Yudao Street, Nanjing 210016, China
[2]Corresponding author
E-mail: [1]*awsxpanda@nuaa.edu.cn*, [2]*ysf@nuaa.edu.cn*, [3]*darcylml@nuaa.edu.cn*, [4]*ywb1987@126.com*
(Received 11 August 2012; accepted 4 December 2012)

Abstract. Dynamic analysis of plate structures based on the Mindlin plate theory has become one of the usual modeling methods for the structural health monitoring (SHM) of composite structures in recent years. Compared to the classical plate theory (CPT) based on Kirchhoff hypothesis, the Mindlin plate theory considers the influence of transverse shear deformation and moment of inertia on displacements. Thus it is more suitable for dynamic analysis of composite laminate with low transverse shear stiffness and large transverse shear deformation. Combining the adhesive layer coupling model of the piezoelectric actuator with the Mindlin plate theory, the dispersion curve of Lamb wave in any direction and mechanical parameters of any point in the composite are obtained, and thus after the substitution of boundary condition, the modeling of piezoelectric wafer excited Lamb wave propagating in composite laminate is realized. The validation experiment is performed on a carbon fiber composite laminate. It proves that the analytical modeling effectively reflects the propagation characteristics of Lamb wave in composite laminate and promotes the engineering application of SHM.

Keywords: Lamb wave, composite laminate, structural health monitoring, dynamic modeling, Mindlin plate theory, piezoelectric ceramic.

Introduction

With the increasing application of composite structures in aerospace engineering, structural health monitoring (SHM) plays an increasingly important role of researches on composite structures [1]. Among the researches, SHM based on active diagnostic Lamb wave and piezoelectric transducers has been a hot spot in recent years [2, 3]. It can be applied to composite laminate extensively applied in aerospace engineering. Thus dynamic modeling of Lamb wave propagating in composite laminate and damage identification and localization based on propagation characteristics of Lamb wave are very important work [4].

Lamb wave is defined as the stress wave that propagates in plates and whose wavelength is with the same order of magnitude as plate thickness. The frequency of Lamb wave used in SHM for composites ranges usually from 20 KHz to 1 MHz and it consists of three kinds of mode: symmetric modes (*S* modes), antisymmetric modes (*A* modes) and shear horizontal modes (*SH* modes). All the three modes of Lamb wave show the characteristics of dispersion and velocity anisotropy in composite laminate. The dispersion characteristic is that the propagation velocity will change with the variation of the central frequency of Lamb wave. The velocity anisotropy in composite laminate means that for the Lamb wave of the same mode and with the same central frequencies, the propagation velocities at different directions are different.

The dispersion and the propagation velocity anisotropy characteristics are first researched in order to model the Lamb wave propagation in composite laminate. However, the modeling is quite difficult because of the complexity and anisotropy of composites. Besides, massive computing resources are consumed for the dynamic modeling of composite laminates. With the development of the computer technology in recent years, many scholars have done lots of

researches about the modeling of Lamb wave in composite laminate. Neau et al [5] derived the dispersion curve of the composite lamina and verified the results with experiments. Yuan [6, 7] analyzed the Lamb wave propagation in composite laminate based on three-dimensional elasticity theory and damage detection and localization were performed based on the modeling result. Rose and Wang [8] obtained the displacement field of isotropic plates surface bonded with circular or rectangular piezoelectric wafers using the Mindlin plate theory. Lowe [9, 10] utilized the global matrix method and the transfer matrix method to analyze the Lamb wave propagation in composite laminate. However, all these researches have to analyze every lamina to obtain the Lamb wave propagation characteristics, which restricts their application in engineering.

The authors propose an analytical modeling method of Lamb wave propagation based on Mindlin plate theory and the model of piezoelectric actuator bonded on laminate through the adhesive layer. Knowing only the engineering mechanical parameter of the composite laminate, the dispersion curve and force distribution in the process of Lamb wave propagation are solved [11]. Then the force distribution is combined with the model of piezoelectric actuator bonded on composite laminate with adhesive layer [12-14]. Through analyzing the equivalent force produced by the piezoelectric actuator with voltage input, the displacement and strain distribution at any point is obtained, and thus the analytical modeling of Lamb wave propagation in composite laminate is realized. Compared to others' researches, the proposed method treats laminate as a material of homogeneous anisotropy, and thus reduces considerably the computation consumption produced by traditional methods and does not need the layup and mechanical parameters of every lamina. The boundary condition is established through the model of piezoelectric actuator bonded on composite laminate with adhesive layer. Finally the displacements and strains at any point in the composite are calculated through theoretical derivation. The obtained results are quite important for the engineering application of composite SHM based on Lamb wave and piezoelectric transducers.

1. Dispersion curve modeling in composite laminate by Mindlin plate theory

1.1 Mindlin plate theory and coordinate definition

The displacement field in the x, y and z directions of a plate based on the two-order Mindlin plate theory can be expressed by:

$$u(x,y,z,t) = u_0(x,y,t) + z\psi_x(x,y,t) + \frac{z^2}{2}\phi_x(x,y,t) \tag{1a}$$

$$v(x,y,z,t) = v_0(x,y,t) + z\psi_y(x,y,t) + \frac{z^2}{2}\phi_y(x,y,t) \tag{1b}$$

$$w(x,y,z,t) = w_0(x,y,t) + z\psi_z(x,y,t) \tag{1c}$$

where u_0, v_0 and w_0 denote the mid-surface displacements at directions x, y and z, respectively. ψ_x and ψ_y denote the rotation angles of the straight line normal to mid-surface before deformation. ψ_z denotes the strain in direction z. ϕ_x and ϕ_y denote partial derivative of ψ_x and ψ_y to z.

Stress and moment resultants per unit length are defined as based on the two-order Mindlin plate theory:

$$(N_x, N_y, N_z, N_{xy}, Q_x, Q_y) = \int_{-h/2}^{h/2} (\sigma_x, \sigma_y, \sigma_z, \sigma_{xy}, \tau_{xy}, \tau_{xz}, \tau_{yz}) dz \tag{2a}$$

$$(M_x, M_y, M_z, M_{xy}, R_x, R_y) = \int_{-h/2}^{h/2} (\sigma_x, \sigma_y, \sigma_z, \sigma_{xy}, \tau_{xy}, \tau_{xz}, \tau_{yz}) z dz \tag{2b}$$

$$(S_x, S_y, S_{xy}) = \int_{-h/2}^{h/2} (\sigma_x, \sigma_y, \sigma_z) z^2 dz \tag{2c}$$

For a laminated composite plate, the stress-strain relation for the monoclinic material with respect to z axis is given by:

$$\begin{Bmatrix} \sigma_1 \\ \sigma_2 \\ \sigma_3 \\ \tau_{23} \\ \tau_{13} \\ \tau_{12} \end{Bmatrix} = \begin{bmatrix} C_{11} & C_{12} & C_{13} & 0 & 0 & 0 \\ C_{12} & C_{22} & C_{23} & 0 & 0 & 0 \\ C_{13} & C_{23} & C_{33} & 0 & 0 & 0 \\ 0 & 0 & 0 & C_{44} & 0 & 0 \\ 0 & 0 & 0 & 0 & C_{55} & 0 \\ 0 & 0 & 0 & 0 & 0 & C_{66} \end{bmatrix} \begin{Bmatrix} \varepsilon_1 \\ \varepsilon_2 \\ \varepsilon_3 \\ \gamma_{23} \\ \gamma_{13} \\ \gamma_{12} \end{Bmatrix} \tag{3}$$

where $\sigma_1, \sigma_2, \sigma_3, \tau_{23}, \tau_{13}, \tau_{12}$ denote the stress components in three directions. $\varepsilon_1, \varepsilon_2, \varepsilon_3, \gamma_{23}, \gamma_{13}, \gamma_{12}$ are the corresponding strain components. C_{ij} is the elastic coefficient. The engineering elastic constant is often used to represent the material elastic property, which includes elasticity modulus E_i, Poisson's ratio ν_{ij} and shear modulus G_{ij}. All these parameters can be obtained by experiment. The relation of the engineering elastic constant and the elastic coefficient is expressed as:

$$\begin{aligned}
&C_{11} = \frac{1-\nu_{23}\nu_{32}}{E_2E_3S}, \quad C_{12} = \frac{\nu_{21}+\nu_{31}\nu_{23}}{E_2E_3S} = \frac{\nu_{12}+\nu_{32}\nu_{13}}{E_1E_3S}, \\
&C_{13} = \frac{\nu_{31}+\nu_{21}\nu_{32}}{E_2E_3S} = \frac{\nu_{13}+\nu_{12}\nu_{23}}{E_1E_2S}, \quad C_{22} = \frac{1-\nu_{13}\nu_{31}}{E_1E_3S}, \\
&C_{23} = \frac{\nu_{32}+\nu_{12}\nu_{31}}{E_1E_3S} = E_3\frac{\nu_{23}+\nu_{21}\nu_{13}}{E_1E_2S}, \quad C_{33} = \frac{1-\nu_{12}\nu_{21}}{E_1E_2S}, \\
&C_{44} = G_{23}, \quad C_{55} = G_{13}, \quad C_{66} = G_{12}, \\
&S = \frac{1-\nu_{12}\nu_{21}-\nu_{23}\nu_{32}-\nu_{31}\nu_{13}-2\nu_{21}\nu_{32}\nu_{13}}{E_1E_2E_3}
\end{aligned} \tag{4}$$

where 1, 2 and 3 denote the three principal directions.

Eq. (1) in conjunction with the strain-displacement relations of classical theory of elasticity leads to the following relations:

$$\varepsilon_x = \varepsilon_{0x} + z\psi_{x,x} + \frac{z^2}{2}\phi_{x,x} \tag{5a}$$

$$\varepsilon_z = \varepsilon_{0z} \tag{5b}$$

$$\varepsilon_y = \varepsilon_{0y} + z\psi_{y,y} + \frac{z^2}{2}\phi_{y,y} \tag{5c}$$

$$\gamma_{xy} = \gamma_{0xy} + z(\psi_{x,y} + \psi_{y,x}) + \frac{z^2}{2}(\phi_{x,y} + \phi_{y,x}) \tag{5d}$$

$$\gamma_{xz} = \gamma_{0xz} + z(\phi_x + \psi_{z,x}) \tag{5e}$$

$$\gamma_{yz} = \gamma_{0yz} + z(\phi_y + \psi_{z,y}) \tag{5f}$$

Substituting eq. (5) into eq. (3) and putting the results into eq. (2) yield the following plate constitutive relations:

$$\begin{Bmatrix} N_x \\ N_y \\ N_z \\ N_{xy} \\ M_x \\ M_y \\ M_{xy} \\ S_x \\ S_y \\ S_{xy} \end{Bmatrix} = \begin{bmatrix} A_{11} & A_{12} & \kappa_3 A_{13} & A_{16} & B_{11} & B_{12} & B_{16} & D_{11}/2 & D_{12}/2 & D_{16}/2 \\ A_{12} & A_{22} & \kappa_3 A_{23} & A_{26} & B_{12} & B_{22} & B_{26} & D_{12}/2 & D_{22}/2 & D_{26}/2 \\ \kappa_3 A_{13} & \kappa_3 A_{23} & \kappa_3^2 A_{33} & \kappa_3 A_{36} & \kappa_3 B_{13} & \kappa_3 B_{23} & \kappa_3 B_{36} & \kappa_3 D_{13}/2 & \kappa_3 D_{23}/2 & \kappa_3 D_{36}/2 \\ A_{16} & A_{26} & \kappa_3 A_{36} & A_{66} & B_{16} & B_{26} & B_{66} & D_{16}/2 & D_{26}/2 & D_{66}/2 \\ B_{11} & B_{12} & \kappa_3 B_{13} & B_{16} & D_{11} & D_{12} & D_{16} & F_{11}/2 & F_{12}/2 & F_{16}/2 \\ B_{12} & B_{22} & \kappa_3 B_{23} & B_{26} & D_{12} & D_{22} & D_{26} & F_{12}/2 & F_{22}/2 & F_{26}/2 \\ B_{16} & B_{26} & \kappa_3 B_{36} & B_{66} & D_{16} & D_{26} & D_{66} & F_{16}/2 & F_{26}/2 & F_{66}/2 \\ D_{11}/2 & D_{12}/2 & \kappa_3 D_{13}/2 & D_{16}/2 & F_{11}/2 & F_{12}/2 & F_{16}/2 & H_{11}/4 & H_{12}/4 & H_{16}/4 \\ D_{12}/2 & D_{22}/2 & \kappa_3 D_{23}/2 & D_{26}/2 & F_{12}/2 & F_{22}/2 & F_{26}/2 & H_{12}/4 & H_{22}/4 & H_{26}/4 \\ D_{16}/2 & D_{26}/2 & \kappa_3 D_{36}/2 & D_{66}/2 & F_{16}/2 & F_{26}/2 & F_{66}/2 & H_{16}/4 & H_{26}/4 & H_{66}/4 \end{bmatrix} \begin{Bmatrix} u_{0,x} \\ v_{0,y} \\ \psi_z \\ u_{0,y}+v_{0,x} \\ \psi_{x,x} \\ \psi_{y,y} \\ \psi_{x,y}+\psi_{y,x} \\ \phi_{x,x} \\ \phi_{y,y} \\ \phi_{x,y}+\phi_{y,x} \end{Bmatrix} \quad (6a)$$

$$\begin{Bmatrix} Q_x \\ Q_y \\ R_x \\ R_y \end{Bmatrix} = \begin{bmatrix} \kappa_1^2 A_{55} & \kappa_1\kappa_2 A_{45} & \kappa_1\kappa_4 B_{55} & \kappa_1\kappa_5 B_{45} \\ \kappa_1\kappa_2 A_{45} & \kappa_2^2 A_{44} & \kappa_2\kappa_4 B_{45} & \kappa_2\kappa_5 B_{44} \\ \kappa_1\kappa_4 B_{55} & \kappa_2\kappa_4 B_{45} & \kappa_4^2 D_{55} & \kappa_4\kappa_5 D_{45} \\ \kappa_1\kappa_5 B_{45} & \kappa_2\kappa_5 B_{44} & \kappa_4\kappa_5 D_{45} & \kappa_5^2 D_{44} \end{bmatrix} \begin{Bmatrix} \psi_x + w_{0,x} \\ \psi_y + w_{0,y} \\ \psi_{z,x} + \phi_x \\ \psi_{z,y} + \phi_y \end{Bmatrix} \quad (6b)$$

where:

$$(A_{ij}B_{ij}D_{ij}F_{ij}H_{ij}) = \int_{-h/2}^{h/2} C_{ij}(1, z, z^2, z^3, z^4)dz$$

h denotes the laminate thickness and κ_i denotes shear correction coefficients: $\kappa_1^2 = \kappa_2^2 = \kappa_3^2 = \pi^2/12$, $\kappa_4^2 = \kappa_5^2 = \pi^2/15$.

1.2 Solution of dispersion curve of Lamb wave based on principle of virtual displacement

With the linear strain-displacement relations, the motion equations of the higher-order theory can be derived using Hamilton's principle [15]:

$$0 = \int_{t_1}^{t_2} (\delta U + \delta V - \delta K)dt \quad (7)$$

where δU is the virtual strain energy, δV is virtual work done by applied force, and δK is the virtual kinetic energy. A set of motion equations are:

$$\frac{\partial N_x}{\partial x} + \frac{\partial N_y}{\partial y} + q_x = I_0 \frac{\partial^2 u_0}{\partial t^2} + \frac{I_2}{2}\frac{\partial^2 \phi_x}{\partial t^2} \quad (8a)$$

$$\frac{\partial N_{xy}}{\partial x} + \frac{\partial N_y}{\partial y} + q_y = I_0 \frac{\partial^2 v_0}{\partial t^2} + \frac{I_2}{2}\frac{\partial^2 \phi_y}{\partial t^2} \quad (8b)$$

$$\frac{\partial Q_x}{\partial x} + \frac{\partial Q_y}{\partial y} + q = I_0 \frac{\partial^2 w_0}{\partial t^2} \quad (8c)$$

$$\frac{\partial M_x}{\partial x} + \frac{\partial M_{xy}}{\partial y} - Q_x + m_x = \frac{I_2}{2}\frac{\partial^2 \psi_x}{\partial t^2} \quad (8d)$$

$$\frac{\partial M_{xy}}{\partial x} + \frac{\partial M_y}{\partial y} - Q_y + m_y = \frac{I_2}{2}\frac{\partial^2 \psi_y}{\partial t^2} \quad (8e)$$

$$\frac{\partial R_x}{\partial x} + \frac{\partial R_y}{\partial y} - N_z + m = I_2 \frac{\partial^2 \psi_z}{\partial t^2} \quad (8f)$$

$$\frac{\partial S_x}{\partial x} + \frac{\partial S_{xy}}{\partial y} - R_z + n_x = \frac{I_0}{2}\frac{\partial^2 u_0}{\partial t^2} + \frac{I_4}{4}\frac{\partial^2 \phi_x}{\partial t^2} \quad (8g)$$

$$\frac{\partial S_{xy}}{\partial x}+\frac{\partial S_y}{\partial y}-R_y+n_y=\frac{I_0}{2}\frac{\partial^2 v_0}{\partial t^2}+\frac{I_4}{4}\frac{\partial^2 \phi_y}{\partial t^2} \tag{8h}$$

where $(I_0, I_1, I_2, I_3, I_4)=\int_{-h/2}^{h/2}\rho(1, z, z^2, z^3, z^4)dz$.

By assuming the solution form as:

$$\begin{aligned} &u_0=U_0e^{i[(k_1x+k_2y)-wt]},\quad v_0=V_0e^{i[(k_1x+k_2y)-wt]},\quad w_0=W_0e^{i[(k_1x+k_2y)-wt]},\\ &\psi_z=\Psi_z e^{i[(k_1x+k_2y)-wt]},\quad \psi_x=\Psi_x e^{i[(k_1x+k_2y)-wt]},\quad \psi_y=\Psi_y e^{i[(k_1x+k_2y)-wt]},\\ &\phi_y=\Phi_y e^{i[(k_1x+k_2y)-wt]},\quad \phi_y=\Phi_y e^{i[(k_1x+k_2y)-wt]}, \end{aligned} \tag{9}$$

substituting eqs. (6) and (9) into eq. (8) yields the following displacement equations of motion:

$$\begin{bmatrix} L_{11} & L_{12} & 0 & L_{14} & L_{15} & L_{16} & L_{17} & L_{18}\\ L_{12} & L_{22} & 0 & L_{15} & L_{25} & L_{26} & L_{18} & L_{28}\\ 0 & 0 & L_{33} & L_{34} & L_{35} & L_{36} & L_{37} & L_{38}\\ L_{14} & L_{15} & L_{34} & L_{44} & L_{45} & L_{46} & L_{47} & L_{48}\\ L_{15} & L_{25} & L_{35} & L_{45} & L_{55} & L_{56} & L_{57} & L_{58}\\ L_{16} & L_{26} & L_{36} & L_{46} & L_{56} & L_{66} & L_{67} & L_{68}\\ L_{17} & L_{18} & L_{37} & L_{47} & L_{57} & L_{67} & L_{77} & L_{78}\\ L_{18} & L_{28} & L_{38} & L_{48} & L_{58} & L_{68} & L_{78} & L_{88} \end{bmatrix}\begin{Bmatrix} U_0\\ V_0\\ W_0\\ \Psi_x\\ \Psi_y\\ \Psi_z\\ \Phi_x\\ \Phi_y \end{Bmatrix}=0 \tag{10}$$

where the coefficients L_{ij} are related with the coefficients A_{ij}, B_{ij}, D_{ij}, F_{ij}, H_{ij}, k_1, k_2, ω and φ.

For symmetric laminates $B_{ij}=F_{ij}=0$, which leads to L_{15}, L_{37}, L_{38}, L_{48}, L_{56} and L_{57} equal to zero, and eq. (10) is decoupled into symmetric waves:

$$\begin{bmatrix} L_{11} & L_{12} & L_{16} & L_{17} & L_{18}\\ L_{12} & L_{22} & L_{26} & L_{18} & L_{28}\\ L_{16} & L_{26} & L_{66} & L_{67} & L_{68}\\ L_{17} & L_{18} & L_{67} & L_{77} & L_{78}\\ L_{18} & L_{28} & L_{68} & L_{78} & L_{88} \end{bmatrix}\begin{Bmatrix} U_0\\ V_0\\ \Psi_z\\ \Phi_x\\ \Phi_y \end{Bmatrix}=0 \tag{11}$$

and antisymmetric waves:

$$\begin{bmatrix} L_{33} & L_{34} & L_{35}\\ L_{34} & L_{44} & L_{45}\\ L_{35} & L_{45} & L_{55} \end{bmatrix}\begin{Bmatrix} W_0\\ \Psi_x\\ \Psi_y \end{Bmatrix}=0 \tag{12}$$

Through solution of eqs. (11) and (12), the phase velocity dispersion curve can be obtained.

2. Piezoelectric actuator model bonded through adhesive layer

2.1 Transversal isotropic piezoelectric material

The piezoelectric transducers aiming at aircraft SHM are usually made of polarized piezoelectric ceramics. They are often cut circular shape and polarized in the thickness direction. In the process of application in SHM, they are often bonded on the surface of

structures and excited by voltage signals. Thus Lamb wave is generated through inverse piezoelectric effect and propagates in structures.

According to Horacio Sosa [12], by introducing the stress function $U(x_1, x_2)$ and complex potential function $\phi_k(z_k) = U_k'(z_k) = dU_k(z_k)/dz_k$ that both satisfy the constitutive equations, the characterisitic of mechanical-electrical coupling of piezoelectric materials can be converted to three complex functions ϕ_1, ϕ_2 and ϕ_3. $z_k = x_1 + \mu_k x_2$, where μ_k are the six conjugate roots of constitutive equations of piezoelectric materials.

To obtain $\phi_k(z_k)$, the following boundary condition is usually assumed:

$$2\Re\sum_{k=1}^{3}\phi_k(z_k) = -\int_0^s t_{2s}ds \tag{13a}$$

$$2\Re\sum_{k=1}^{3}\mu_k\phi_k(z_k) = \int_0^s t_{1s}ds \tag{13b}$$

$$2\Re\sum_{k=1}^{3}\lambda_k\phi(z_k) = -\int_0^s D_n ds \tag{13c}$$

where t_{1s} and t_{2s} denote the force applied to piezoelectric materials in directions x_1 and x_2, s denotes the arc of the circular shape piezoelectric wafer. D_n denotes the electric displacement component normal to the surface of piezoelectric wafer. λ_k is a parameter decided by piezoelectric material coefficient and μ_k. $\Re$ denotes the real part operator.

2.2 Actuator model of piezoelectric materials

The working principle of a piezoelectric wafer of thickness t_a bonded on the surface of a plate structure is shown in Fig. 1. When voltage signals are applied on two poles of a piezoelectric wafer, it will deform due to the inverse piezoelectric effect. The adhesive layer with the thickness t_b will pass the deformation from the piezoelectric wafer to the plate surface and act as the excitation.

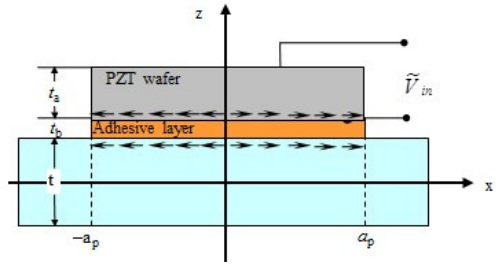

Fig. 1. The bonding of piezoelectric wafer and plate structure

According to E. F. Crawley [13], the mechanical effect of the actuator model can be expressed as:

$$\frac{\tau}{E} = -\frac{1}{t_b}\frac{G_b}{G_a}\frac{E_a}{E\Gamma}\left(\frac{\sinh\Gamma\overline{x}}{\cosh\Gamma}\right)\Lambda$$

$$\Gamma^2 = \frac{G_b}{E_a}\frac{1}{t_a t_b}\left(\frac{\Psi+\alpha}{\Psi}\right) \tag{14}$$

$$\Psi = \frac{Et}{E_a t_a}$$

where $\bar{x}$ is the dimensionless coordinate of x, $\bar{x} \in [-1,1]$, τ denotes the shear stress passed from the adhesive layer to the plate structure. The subscript a and b of the elastic modulus E, shear modulus G and thickness t refer to the piezoelectric wafer and the adhesive layer, respectively. The three kinds of variables without any subscript refer to the plate structure. Λ denotes the strain caused by the inverse piezoelectric effect, Γ denotes the shear damping, Ψ denotes the relative stiffness and α denotes the Euler-Bernoulli coefficient and is set to be 4 in this study.

Substituting Γ with different values, the obtained shear stresses are plotted in Fig. 2. It can be concluded that when Γ is large enough, the actuating effect can be equivalent to distributed shear force only on the edge of the piezoelectric wafer. Thus eq. (14) can be simplified as:

$$\frac{\tau(x)}{E} = -\frac{1}{t_b}\frac{G_b}{G_a}\frac{E_a}{E\Gamma}\Lambda\left[\delta(x-a)-\delta(x+a)\right] \tag{15}$$

where $\delta(x)$ denotes Dirac function that $\delta(x=0)=1$ and $\delta(x\neq 0)=0$.

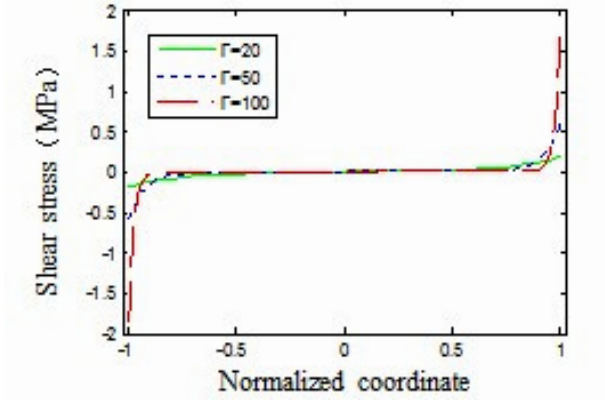

Fig. 2. Shear stress pass from piezoelectric actuator to adhesive layer

Substituting the constraint condition of the adhesive layer in eq. (15) into the boundary condition of piezoelectric wafer in eq. (13), the mechanical-electrical coupling field of the actuator can be analytically expressed as:

$$\begin{aligned}\tau_a(x) &= a\tau_0\left[\delta(x-a)-\delta(x+a)\right] \\ &= -\frac{a}{t_b}\frac{G_b}{G_a}\frac{E_a}{\Gamma}\frac{b_{21}\tilde{V}(\omega)}{\delta_{22}t_a}\left[\delta(x-a)-\delta(x+a)\right]\end{aligned} \tag{16}$$

where $\tilde{V}(\omega)$ denotes the actuating AC voltage, τ_0 denotes the distributed shear force value on the edge of the piezoelectric wafer. b_{21} and δ_{22} are the piezoelectric constants.

2.3 Boundary condition of piezoelectric actuator

When the piezoelectric actuator is bonded on the surface of isotropic plate structures, the research object can be simplified as a two dimensional plain strain problem. However, for the

anisotropy characteristics of composite structures, a fully three dimensional dynamic analysis shown in Fig. 3 is necessary.

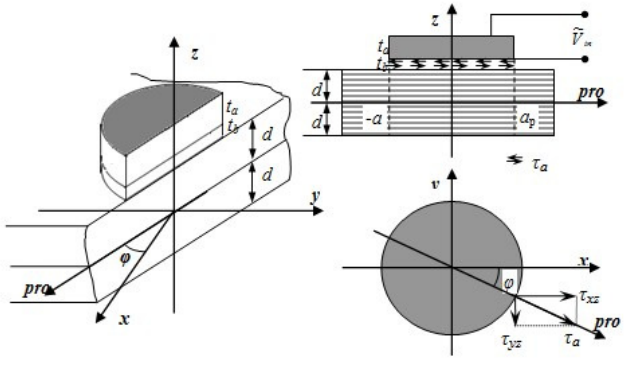

Fig. 3. Actuator model for composite laminate

As described previously, the effect of the piezoelectric actuator can be equivalent to a shear force along the radial direction, resulting in the radial propagation of Lamb wave. Now the propagation direction with an angle φ to axis x is researched. A shear stress τ_a in the propagation direction can be divided into two components τ_{xz} and τ_{yz}, where $\tau_{xz} = \tau_a \cos\phi$ and $\tau_{yz} = \tau_a \sin\phi$.

According to Giurgiutiu [17], the shear stress on the single surface of a plate can be divided into the shear stresses on both surfaces that excite two modes of Lamb waves independently: symmetric Lamb wave and antisymmetric Lamb wave, which are shown in Fig. 4.

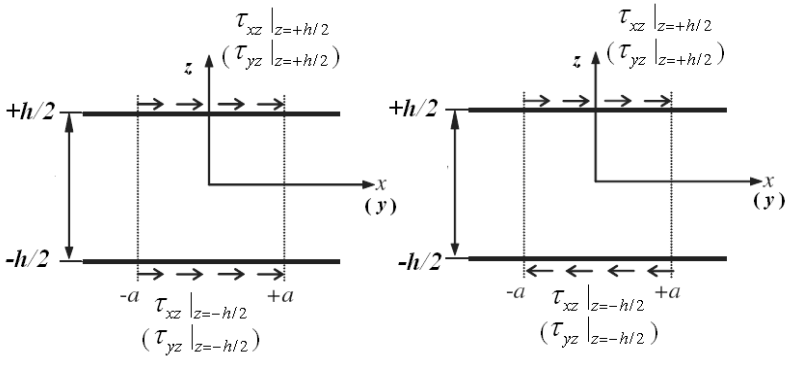

(a) (b)

Fig. 4. Shear stress decomposition into (a) symmetric mode and (b) antisymmetric mode

The boundary condition of the plate structure at the actuator location in the spatial domain is derived. The symmetric mode is expressed as:

$$\begin{cases} u\big|_{z=-h/2} = u\big|_{z=h/2}, \ v\big|_{z=-h/2} = v\big|_{z=h/2} \\ \tau_{xz}\big|_{z=-h/2} = -\tau_{xz}\big|_{z=h/2} = -\dfrac{1}{2}\tau_{xz}, \ \tau_{yz}\big|_{z=-h/2} = -\tau_{yz}\big|_{z=h/2} = -\dfrac{1}{2}\tau_{yz} \\ w\big|_{z=-h/2} = -w\big|_{z=h/2} \\ \sigma_z\big|_{z=h/2} = -\sigma_z\big|_{z=h/2} = 0 \end{cases} \tag{17a}$$

and the antisymmetric mode is expressed as:

$$\begin{cases} u\big|_{z=-h/2} = -u\big|_{z=h/2}, \quad v\big|_{z=-h/2} = -v\big|_{z=h/2} \\ \tau_{xz}\big|_{z=-h/2} = \tau_{xz}\big|_{z=h/2} = \dfrac{1}{2}\tau_{xz}, \quad \tau_{yz}\big|_{z=-h/2} = \tau_{yz}\big|_{z=h/2} = \dfrac{1}{2}\tau_{yz} \\ w\big|_{z=-h/2} = w\big|_{z=h/2} \\ \sigma_z\big|_{z=h/2} = -\sigma_z\big|_{z=h/2} = 0 \end{cases} \tag{17b}$$

Combining the boundary condition in eq. (17) and the dynamic analysis of composite laminate based on Mindlin plate theory, the analytical modeling of Lamb wave in composite laminate is realized.

3. Piezoelectric actuator effect analysis

3.1 Application of the piezoelectric actuator boundary condition

A sinusoidal signal is assumed to be the excitation $\tilde{V}_{in}(\omega) = V_{in0} \cdot e^{-i\omega t}$. The shear stress between the adhesive layer and the plate structures can be divided into:

$$\tau_{xz}(x,\omega) = -\frac{1}{t_b}\frac{G_b}{G_a}\frac{E_a}{\Gamma}\frac{b_{21}Et}{\delta_{22}t_a}V_{in0}\cos\phi\left[\delta(x/\cos\phi - a) - \delta(x/\cos\phi + a)\right]\cdot e^{-i\omega t} \tag{18a}$$

$$\tau_{yz}(y,\omega) = -\frac{1}{t_b}\frac{G_b}{G_a}\frac{E_a}{\Gamma}\frac{b_{21}Et}{\delta_{22}t_a}V_{in0}\sin\phi\left[\delta(y/\sin\phi - a) - \delta(y/\sin\phi + a)\right]\cdot e^{-i\omega t} \tag{18b}$$

The signal in spatial domain is often converted to the wavenumber domain for convenience. The respective wavenumbers k_1 and k_2 in directions x and y are required because of the anisotropy property of composite laminate. The process of conversion from x-y space to k_1-k_2 space is realized through Fourier transform:

$$\begin{aligned} \tilde{f}(k_1) &= \int_{-\infty}^{+\infty} f(x)e^{-ik_1x}dx \\ \tilde{f}(k_2) &= \int_{-\infty}^{+\infty} f(y)e^{-ik_2y}dy \\ f(x) &= \frac{1}{2\pi}\int_{-\infty}^{+\infty} \tilde{f}(k_1)e^{ik_1x}dk_1 \\ f(y) &= \frac{1}{2\pi}\int_{-\infty}^{+\infty} \tilde{f}(k_2)e^{ik_2y}dk_2 \end{aligned} \tag{19}$$

The shear stress excitation in eq. (18) is converted to:

$$\begin{aligned} \tilde{\tau}_{xz}(k_1) &= \int_{-\infty}^{+\infty} \tau_0\cos\phi\left[\delta(x/\cos\phi - a) - \delta(x/\cos\phi + a)\right]e^{-ik_1x}dx \\ &= a\tau_0\cos\phi[-2i\sin(ak_1\cos\phi)] \end{aligned} \tag{20a}$$

$$\begin{aligned} \tilde{\tau}_{yz}(k_2) &= \int_{-\infty}^{+\infty} \tau_0\cos\phi\left[\delta(y/\sin\phi - a) - \delta(y/\sin\phi + a)\right]e^{-ik_2y}dy \\ &= a\tau_0\sin\phi[-2i\sin(ak_2\sin\phi)] \end{aligned} \tag{20b}$$

To simply the deduction process, only the symmetric mode is illustrated for example. The deduction for the antisymmetric can be realized with the same process as the symmetric mode.

Substituting the shear stress excitation in eq. (20) to the boundary condition in eq. (17), the boundary condition for the symmetric mode in space domain is expressed as:

$$\begin{cases} \tilde{u}\big|_{z=-h/2} = \tilde{u}\big|_{z=h/2}, \ \tilde{v}\big|_{z=-h/2} = \tilde{v}\big|_{z=h/2} \\ \tilde{\tau}_{xz}\big|_{z=-h/2} = -\tilde{\tau}_{xz}\big|_{z=h/2} = -\frac{1}{2}\tilde{\tau}_{xz} = -\frac{1}{2}a\tau_0\cos\phi[-2i\sin(ak_1\cos\phi)] \\ \tilde{\tau}_{yz}\big|_{z=-h/2} = -\tilde{\tau}_{yz}\big|_{z=h/2} = -\frac{1}{2}\tilde{\tau}_{yz} = -\frac{1}{2}a\tau_0\sin\phi[-2i\sin(ak_2\sin\phi)] \\ \tilde{w}\big|_{z=-h/2} = -\tilde{w}\big|_{z=h/2} \\ \tilde{\sigma}_z\big|_{z=h/2} = -\tilde{\sigma}_z\big|_{z=h/2} = 0 \end{cases} \tag{21}$$

Substituting the boundary condition in eq. (21) into the basic displacement expression in eq. (1), the following relations can be obtained:

$$\tilde{\psi}_x(k_1) = 0, \ \tilde{\psi}_y(k_2) = 0, \ \tilde{w}_0 = 0 \tag{22}$$

Substituting the boundary condition in eqs. (22) and eq. (21) into eq. (2), it can be obtained:

$$\begin{aligned} \tilde{Q}_x(k_1) &= \int_{-h/2}^{h/2}\tilde{\tau}_{xz}dz = 0 \\ \tilde{Q}_y(k_2) &= \int_{-h/2}^{h/2}\tilde{\tau}_{yz}dz = 0 \\ \tilde{R}_x(k_1) &= \int_{-h/2}^{h/2}\tilde{\tau}_{xz}zdz = \frac{1}{16}ah^2\tau_0\cos\phi[-2i\sin(ak_1\cos\phi)] \\ \tilde{R}_y(k_2) &= \int_{-h/2}^{h/2}\tilde{\tau}_{yz}zdz = \frac{1}{16}ah^2\tau_0\sin\phi[-2i\sin(ak_2\sin\phi)] \end{aligned} \tag{23}$$

Substituting eqs. (21), (22) and (23) into the constitutive eq. (6), it can be derived that:

$$\begin{aligned} \tilde{Q}_x &= \kappa_1\kappa_4 B_{55}\left(\tilde{\psi}_{z,x} + \tilde{\phi}_x\right) + \kappa_1\kappa_5 B_{45}\left(\tilde{\psi}_{z,y} + \tilde{\phi}_y\right) = 0 \\ \tilde{Q}_y &= \kappa_2\kappa_4 B_{45}\left(\tilde{\psi}_{z,x} + \tilde{\phi}_x\right) + \kappa_2\kappa_5 B_{44}\left(\tilde{\psi}_{z,y} + \tilde{\phi}_y\right) = 0 \\ \tilde{R}_x &= \kappa_4^2 D_{55}\left(\tilde{\psi}_{z,x} + \tilde{\phi}_x\right) + \kappa_4\kappa_5 D_{45}\left(\tilde{\psi}_{z,y} + \tilde{\phi}_y\right) \\ &= \frac{1}{16}ah^2\tau_0\cos\phi[-2i\sin(ak_1\cos\phi)] \\ \tilde{R}_y &= \kappa_4\kappa_5 D_{45}\left(\tilde{\psi}_{z,x} + \tilde{\phi}_x\right) + \kappa_5^2 D_{44}\left(\tilde{\psi}_{z,y} + \tilde{\phi}_y\right) \\ &= \frac{1}{16}ah^2\tau_0\sin\phi[-2i\sin(ak_2\sin\phi)] \end{aligned} \tag{24a}$$

Following the same process above for the antisymmetric mode, it can be obtained for the antisymmetric mode that:

$$\begin{aligned} \tilde{Q}_x &= \kappa_1^2 A_{55}\left(\tilde{\psi}_x + \tilde{w}_{0,x}\right) + \kappa_1\kappa_2 A_{45}\left(\psi_y + \tilde{w}_{0,y}\right) \\ &= \frac{1}{2}ah\tau_0\cos\phi[-2i\sin(ak_1\cos\phi)] \end{aligned}$$

$$\begin{aligned}\widetilde{Q}_y &= \kappa_1\kappa_2 A_{45}\left(\widetilde{\psi}_x + \widetilde{w}_{0,x}\right) + \kappa_2{}^2 A_{44}\left(\widetilde{\psi}_y + \widetilde{w}_{0,y}\right) \\ &= \frac{1}{2}ah\tau_0 \sin\phi[-2i\sin(ak_2\sin\phi)] \\ \widetilde{R}_x &= \kappa_1\kappa_4 B_{55}\left(\widetilde{\psi}_x + \widetilde{w}_{0,x}\right) + \kappa_2\kappa_4 B_{45}\left(\widetilde{\psi}_y + \widetilde{w}_{0,y}\right) = 0 \\ \widetilde{R}_y &= \kappa_1\kappa_5 B_{45}\left(\widetilde{\psi}_x + \widetilde{w}_{0,x}\right) + \kappa_2\kappa_5 B_{44}\left(\widetilde{\psi}_y + \widetilde{w}_{0,y}\right) = 0\end{aligned} \tag{24b}$$

The right side of eqs. (8c) and (8f) can be rewritten as:

$$I_0\frac{\partial^2 w_0}{\partial t^2} = -\omega^2 W_0 e^{i[(k_1x+k_2y)-\omega t]}, \quad I_2\frac{\partial^2 \psi_z}{\partial t^2} = -\omega^2\Psi_z e^{i[(k_1x+k_2y)-\omega t]} \tag{25}$$

In the condition that no loads are applied and only the single piezoelectric wafer is actuated for Lamb wave propagation in composite laminate, the body forces q and m are both equal to zero. However, it can be seen in eq. (6) that the force N_z in eq. (8f) is composed of many components, most of which are related to the first derivatives of displacements and rotation angles to x and y. Thus considering the small deformation of Lamb wave propagation in composite laminate, these derivatives are negligible compared to ψ_z and then N_z is simplified as $N_z = k_3{}^2 A_{33}\psi_z$ while solving eq. (8f).

Only taking the key amplitude terms W_0 and Ψ_z from w_0 and ψ_z into consideration, they can be expressed with Q_x, Q_y, R_x and R_y as:

$$W_0 = \frac{\dfrac{\partial Q_x}{\partial x} + \dfrac{\partial Q_y}{\partial y}}{-\omega^2 I_0} \tag{26a}$$

$$\Psi_z = \frac{\dfrac{\partial R_x}{\partial x} + \dfrac{\partial R_y}{\partial y}}{1-\omega^2 I_0} \tag{26b}$$

Considering the derivate property of Fourier transform, the following equations can be obtained by converting eq. (26a) to the wavenumber domain:

$$\tilde{W}_0(k_1, y) = \frac{ik_1\tilde{Q}_x(k_1) + \dfrac{\partial Q_y}{\partial y}}{-\omega^2 I_0} \tag{27a}$$

$$\tilde{W}_0(x, k_2) = \frac{\dfrac{\partial Q_x}{\partial x} + ik_2\tilde{Q}_y(k_2)}{-\omega^2 I_0} \tag{27b}$$

$$\tilde{\Psi}_z(k_1, y) = \frac{ik_1\tilde{R}_x(k_1) + \dfrac{\partial R_y}{\partial y}}{1-\omega^2 I_0} \tag{27c}$$

$$\tilde{\Psi}_z(x, k_2) = \frac{\dfrac{\partial R_x}{\partial x} + ik_2\tilde{R}_y(k_2)}{1-\omega^2 I_0} \tag{27d}$$

According to the inverse Fourier transform in eq. (19), the internal forces Q_x, Q_y, R_x and R_y can be substituted with corresponding variables in space domain, and thus W_0 and Ψ_z can be expressed in wavenumber domain as:

$$\Psi_z(x,y) = \frac{\dfrac{\partial R_x}{\partial x} + \dfrac{\partial R_y}{\partial y}}{1-\omega^2 I_0} = \frac{ik_1\widetilde{R_x}(k_1) + ik_2\widetilde{R_y}(k_2)}{1-\omega^2 I_0} \tag{28a}$$

$$= \frac{ah^2\tau_0}{8(1-\omega^2 I_0)}\left[k_{xS0}\cos\phi\sin(ak_{xS0}\cos\phi) + k_{yS0}\sin\phi\sin(ak_{yS0}\sin\phi)\right]$$

$$W_0(x,y) = \frac{\dfrac{\partial Q_x}{\partial x} + \dfrac{\partial Q_y}{\partial y}}{-\omega^2 I_0} = \frac{ik_1\widetilde{Q_x}(k_1) + ik_2\widetilde{Q_y}(k_2)}{-\omega^2 I_0} \tag{28b}$$

$$= \frac{ah\tau_0}{-\omega^2 I_0}\left[k_{xA0}\cos\phi\sin(ak_{xA0}\cos\phi) + k_{yA0}\sin\phi\sin(ak_{yA0}\sin\phi)\right]$$

3.2 Solution of dispersion curve of Lamb wave in wavenumber domain

Section 1.2 gives the dispersion eqs. (11) and (12), among which the coefficients L_{ij} are functions of k_x, k_y, ω and φ. W_0 and Ψ_z have already been solved in section 2.1. Thus the other six unknows in dispersion eqs. (11) and (12) can be obtained through solving the linear set of equations.

Solving eq. (11) by putting Ψ_z to the right side:

$$\begin{bmatrix} L_{11} & L_{12} & L_{17} & L_{18} \\ L_{12} & L_{22} & L_{18} & L_{28} \\ L_{16} & L_{26} & L_{67} & L_{68} \\ L_{17} & L_{18} & L_{77} & L_{78} \\ L_{18} & L_{28} & L_{78} & L_{88} \end{bmatrix} \begin{Bmatrix} U_0 \\ V_0 \\ \Phi_x \\ \Phi_y \end{Bmatrix} = -\begin{bmatrix} L_{16} \\ L_{26} \\ L_{66} \\ L_{67} \\ L_{68} \end{bmatrix} \Psi_z \tag{29}$$

Eq. (29) can be easily solved and U_0, V_0, Φ_x and Φ_y can be expressed with Ψ_z and are all proportional to Ψ_z. The respective ratios are expressed as $R_{U\Psi}$, $R_{V\Psi}$, $R_{X\Psi}$ and $R_{Y\Psi}$.

In a similar way, Ψ_x and Ψ_y in eq. (12) can be also solved by putting Ψ_z to the right side. The respective ratios are expressed as R_{XW} and R_{YW}.

Thus the six displacement unknown components can all be expressed with Q_x, Q_y, R_x and R_y in wavenumber domain, among which the symmetric displacements are only related to R_x and R_y, and antisymmetric displacements are only related to Q_x and Q_y. With the solved six displacement components of composite laminate in the process of Lamb wave propagation, the transient displacements in the mid-surface at any time can be obtained as:

$$u_0 = U_0 e^{i[(k_1x+k_2y)-wt]} = -R_{U\Psi}\frac{ik_1\widetilde{R_x}(k_1) + ik_2\widetilde{R_y}(k_2)}{1-\omega^2 I_0}e^{i[(k_1x+k_2y)-wt]} \tag{30a}$$

$$v_0 = V_0 e^{i[(k_1x+k_2y)-wt]} = -R_{V\Psi}\frac{ik_1\widetilde{R}_x(k_1)+ik_2\widetilde{R}_y(k_2)}{1-\omega^2 I_0}e^{i[(k_1x+k_2y)-wt]} \tag{30b}$$

$$w_0 = W_0 e^{i[(k_1x+k_2y)-wt]} = \frac{ik_1\widetilde{Q}_x(k_1)+ik_2\widetilde{Q}_y(k_2)}{-\omega^2 I_0}e^{i[(k_1x+k_2y)-wt]} \tag{30c}$$

$$\psi_x = \Psi_x e^{i[(k_1x+k_2y)-wt]} = R_{XW}\frac{ik_1\widetilde{Q}_x(k_1)+ik_2\widetilde{Q}_y(k_2)}{-\omega^2 I_0}e^{i[(k_1x+k_2y)-wt]} \tag{30d}$$

$$\psi_y = \Psi_y e^{i[(k_1x+k_2y)-wt]} = R_{Y\Psi}\frac{ik_1\widetilde{Q}_x(k_1)+ik_2\widetilde{Q}_y(k_2)}{-\omega^2 I_0}e^{i[(k_1x+k_2y)-wt]} \tag{30e}$$

$$\psi_z = \Psi_z e^{i[(k_1x+k_2y)-wt]} = \frac{ik_1\widetilde{R}_x(k_1)+ik_2\widetilde{R}_y(k_2)}{1-\omega^2 I_0}e^{i[(k_1x+k_2y)-wt]} \tag{30f}$$

$$\phi_x = \Phi_x e^{i[(k_1x+k_2y)-wt]} = -R_{X\Psi}\frac{ik_1\widetilde{R}_x(k_1)+ik_2\widetilde{R}_y(k_2)}{1-\omega^2 I_0}e^{i[(k_1x+k_2y)-wt]} \tag{30g}$$

$$\phi_y = \Phi_y e^{i[(k_1x+k_2y)-wt]} = -R_{Y\Psi}\frac{ik_1\widetilde{R}_x(k_1)+ik_2\widetilde{R}_y(k_2)}{1-\omega^2 I_0}e^{i[(k_1x+k_2y)-wt]} \tag{30h}$$

Substituting $z = h/2$ into eq. (1), the displacements and strains on the upper surface can be expressed as:

$$u(x,y,t)\big|_{z=h/2} = u_0(x,y,t)+\frac{h}{2}\psi_x(x,y,t)+\frac{h^2}{8}\phi_x(x,y,t) \tag{31a}$$

$$v(x,y,t)\big|_{z=h/2} = v_0(x,y,t)+\frac{h}{2}\psi_y(x,y,t)+\frac{h^2}{8}\phi_y(x,y,t) \tag{31b}$$

$$w(x,y,t)\big|_{z=h/2} = w_0(x,y,t)+\frac{h}{2}\psi_z(x,y,t) \tag{31c}$$

$$\varepsilon_x(x,y,t)\big|_{z=h/2} = u_0(x,y,t)_{,x}+\frac{h}{2}\psi_x(x,y,t)_{,x}+\frac{h^2}{8}\phi_x(x,y,t)_{,x} \tag{31d}$$

$$\varepsilon_y(x,y,t)\big|_{z=h/2} = v_0(x,y,t)_{,y}+\frac{h}{2}\psi_y(x,y,t)_{,y}+\frac{h^2}{8}\phi_y(x,y,t)_{,y} \tag{31e}$$

$$\begin{aligned}\gamma_{xy}(x,y,t)\big|_{z=h/2} &= u_0(x,y,t)_{,y}+v_0(x,y,t)_{,x}+\frac{h}{4}\left[\psi_x(x,y,t)_{,y}+\psi_y(x,y,t)_{,x}\right]\\ &+\frac{h^2}{8}\left[\phi_x(x,y,t)_{,y}+\phi_y(x,y,t)_{,x}\right]\end{aligned} \tag{31f}$$

The final expressions of displacements and strains are obtained according to the above derivation.

4. Theoretical results and experimental validation

4.1 Experiment setup

As shown in Fig. 5, thirty-six PZT wafers P1 to P36 are surfaced bonded on the composite laminate mentioned above and constitute a circle with an equal angle 10^0 each other. In the

center of the thirty-six PZT wafers, another PZT wafer P37 is bonded to act as the actuator, while others as the sensors. The details of the composite laminate and the PZT wafer placement are both shown in Fig. 6. The CF/EP composite laminate is manufactured with 18 plies with the sequence of $[45/0/-45/90/0/-45/0/-45/0]_S$ with the dimensions 600 mm×600 mm×2.16 mm. The whole mechanical property of the laminate is listed in Table 1.

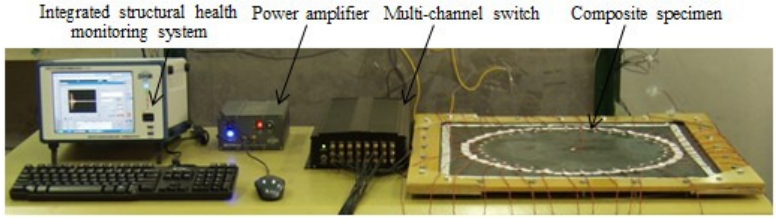

Fig. 5. Experiment system illustration

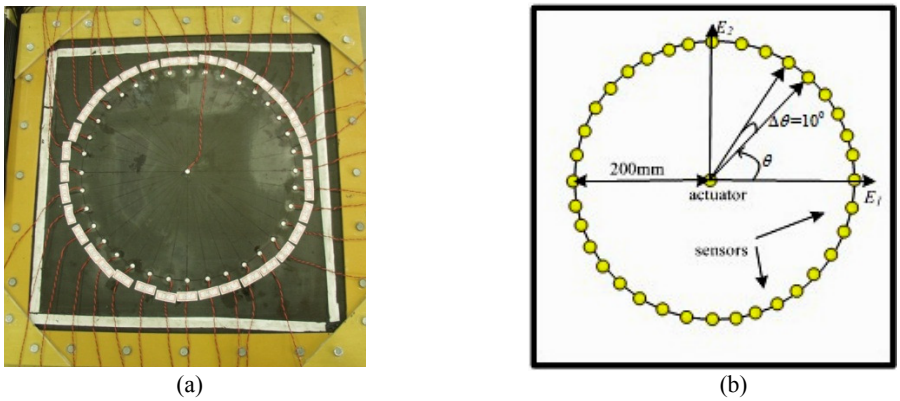

(a) (b)

Fig. 6. Placement of piezoelectric wafer:
(a) composite laminate and piezoelectric wafer, (b) geometric illustration of piezoelectric placement

Table 1. Mechanical parameters of the composite laminate

ρ (kg·m^{-3})	E_1 (GPa)	E_2 (GPa)	E_3 (GPa)	G_{12} (GPa)	G_{13} (GPa)	G_{23} (GPa)	μ_{12}	μ_{13}	μ_{23}	h (mm)
1.61×10^3	73.068	34.443	19.4326	17.941	44.7	44.7	0.4328	0.2318	0.2673	2.25

Shown in Fig. 6, the experiment is done through the integrated structural health monitoring system designed by the Aeronautical Science Key Laboratory for Smart Materials and Structures in Nanjing University of Aeronautics and Astronautics.

4.2 Theoretical phase velocity and group velocity

The phase velocity dispersion curve at direction E_1 for the three kinds of mode calculated from eqs. (11) and (12) are as shown in Fig. 7. The group velocity is calculated as:

$$c_g = \frac{c_p^{\ 2}}{c_p - f\dfrac{dc_p}{df}} \tag{32}$$

where c_p and f denote the phase velocity and the corresponding frequency.

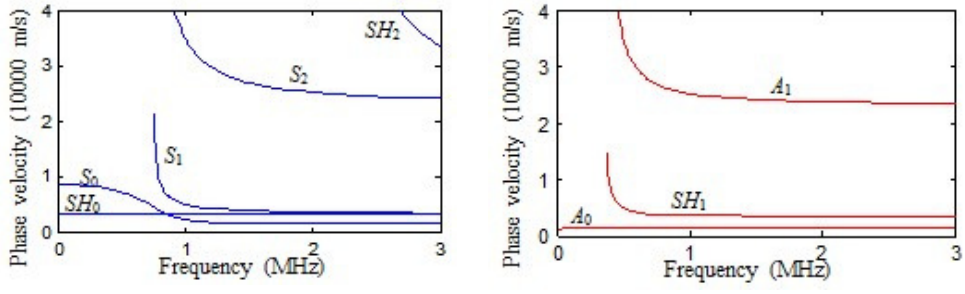

(a) (b)

Fig. 7. Dispersion curve of phase velocity in direction E_1: (a) symmetric mode, (b) antisymmetric mode

The group velocity dispersion curve at direction E_1 for the three kinds of mode calculated from eqs. (11) and (12) are as shown in Fig. 8. As to the applied order of the Mindlin plate theory, a 5×5 matrix and 3×3 matrix are solved for the symmetric modes and antisymmetric modes, respectively. With the increase of the order, more modes can be calculated.

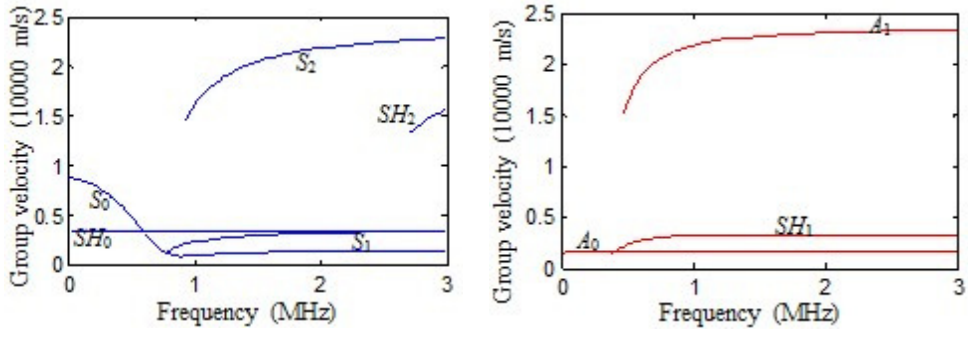

(a) (b)

Fig. 8. Dispersion curve of group velocity in direction E_1: (a) symmetric mode, (b) antisymmetric mode

The group velocities of Lamb wave in different directions under the frequency of 2.9 MHz are given in Fig. 9. For the anisotropy property of the composite laminate, Lamb wave propagates at different directions with different velocities.

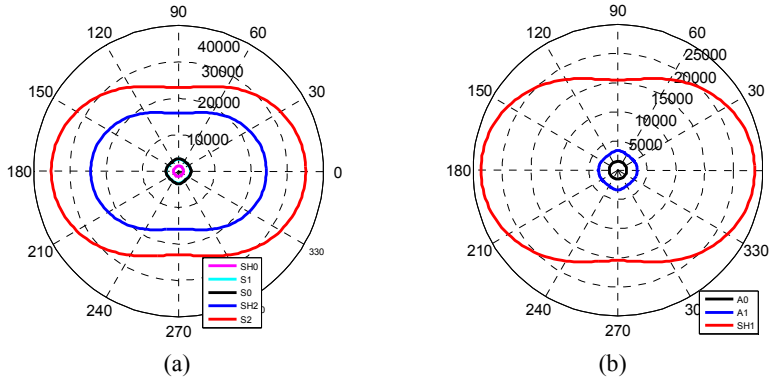

(a) (b)

Fig. 9. Group velocities of Lamb wave in different directions under the frequency of 2.9MHz: (a) symmetric mode, (b) antisymmetric mode

4.3 Group velocity comparison

A modulated five-cycle sine burst with a certain central frequency usually is adopted to excite diagnostic waves into the laminate. Fig. 10 shows the waveform and the corresponding power spectrum. The response signals in direction E_1 under different excitation frequencies are as shown in Fig. 11, where EMI is short for electromagnetic interference, S_0 and A_0 denote the fundamental symmetric and antisymmetric mode, respectively. The former propagates faster than the latter. Besides, the amplitude of the former is close to zero under frequencies lower than 100 KHz, then the amplitude increases rapidly till the frequency around 400 KHz, and finally it decreases under the frequencies from 400 KHz to 500 KHz. As to the fundamental antisymmetric mode A_0, the amplitudes are obvious only under frequencies of 200 KHz. Since A_0 mode has a lower velocity than S_0 mode, reflection of S_0 mode from the boundary will interfere the direct arrival wave of A_0, which influences the exact calculation of group velocity of A_0 mode. Thus, according to the above discussion, the group velocity comparison based on the Mindlin plate theory and the experiment are performed under frequency range from 20 KHz to 200 KHz and from 200 KHz to 500 KHz for A_0 mode and S_0 mode, respectively.

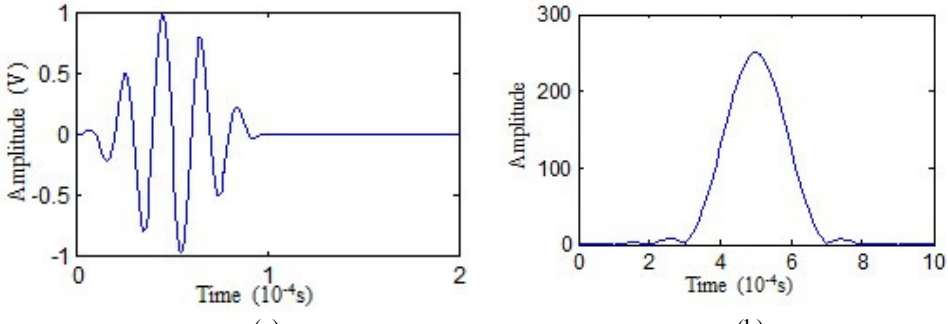

(a) (b)

Fig. 10. Modulated sine wave: (a) original signals, (b) power spectrum

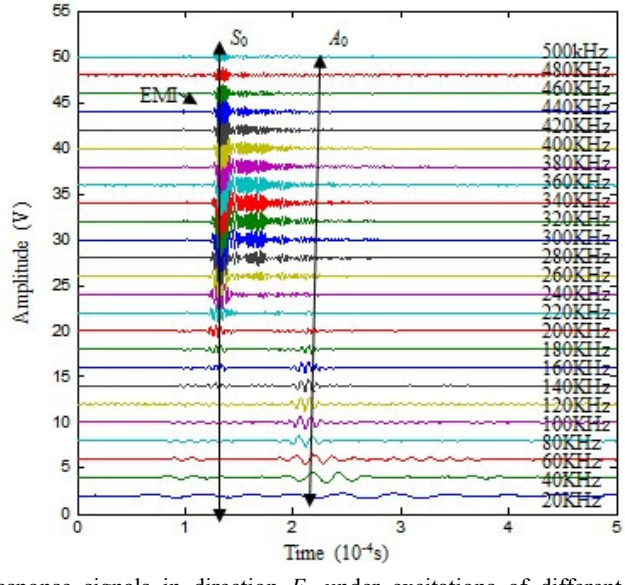

Fig. 11. Response signals in direction E_1 under excitations of different frequencies

Complex Shannon wavelet transform is used here to extract the wave envelop from the original wave form. The signals before and after Complex Shannon wavelet transform are shown in Fig. 12, which also illustrates how to calculate the group velocity by response signals from the experiment. In Fig. 12(b), t_0 and t_1 correspond to the time with the maximum amplitudes of the acting signal and response signal after Complex Shannon wavelet transform. The Lamb wave time-of-flight is $t_1 - t_0$. Thus, the group velocity can be obtained by:

$$c_g = \frac{s}{t_1 - t_0} \tag{33}$$

where s is the distance between the actuator and the sensor.

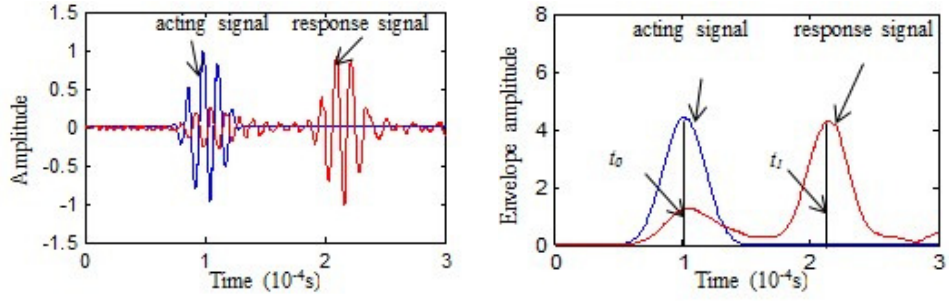

(a) (b)

Fig. 12. Group velocity calculation:
(a) original signals, (b) wave envelopes obtained after Shannon wavelet transform

The group velocities of A_0 mode and S_0 mode are compared in directions E_1 and E_2, which are shown in Fig. 13. For A_0 mode, the theoretical value correlates quite well with the experiment results. However, only the theoretical value from 210 KHz to 400 KHz correlate well with the experiment results and a considerable difference between the theory and experiment results is observed in the frequency range of 410 KHz to 500 KHz. This phenomenon can be explained by the following reasons: the 2nd order Mindlin plate theory is accurate enough for the solution of dispersion characteristics under the frequency below about 400 KHz, but a higher order is necessary for accurate modeling above 400 KHz.

Another phenomenon observed from Fig. 13 is the obvious group velocity differences in direction E_1 and E_2. Since the elastic modulus in direction E_1 is larger than that in direction E_2, the group velocity in direction E_1 is larger than that in direction E_2. In many damage monitoring algorithms that utilize the time domain information to localize damage, the velocity differences in different directions should be addressed.

The last phenomenon is Lamb wave propagates with multi-modes. Two fundamental modes A_0 mode and S_0 mode always exist in the plate. With the increase of the frequency, more modes will appear in the surface, which significantly complicates the wave propagation in the plate. Thus the comparison of theory value and experiment result is performed under frequencies below 500 KHz to ensure only A_0 mode and S_0 mode exist in the plate.

4.4 Direct arrival wave amplitude comparison

Since A_0 mode is mainly composed of flexural wave with out-of-surface displacement, the displacement w is extracted for the A_0 mode amplitude comparison. Similarly, S_0 mode is mainly composed of longitudinal wave with in-surface displacement, the displacement u is extracted for the S_0 mode amplitude comparison. Fig. 14 gives the normalized amplitude

comparison between the theory values and experiment results in direction E_1. The experiments show the amplitude of the A_0 mode reaches the maximum under the frequency 130 KHz and S_0 mode reaches the maximum under the frequency 330 KHz. As to the theory calculation, A_0 mode and S_0 mode reach the maximums under the frequency 150 KHz and 300 KHz, respectively. The correlation of the frequencies corresponding to the two modes' maximum amplitudes and the amplitude variation trends between the theory calculation and experiment results show the effectiveness of the proposed analytical modeling based on Mindlin plate theory.

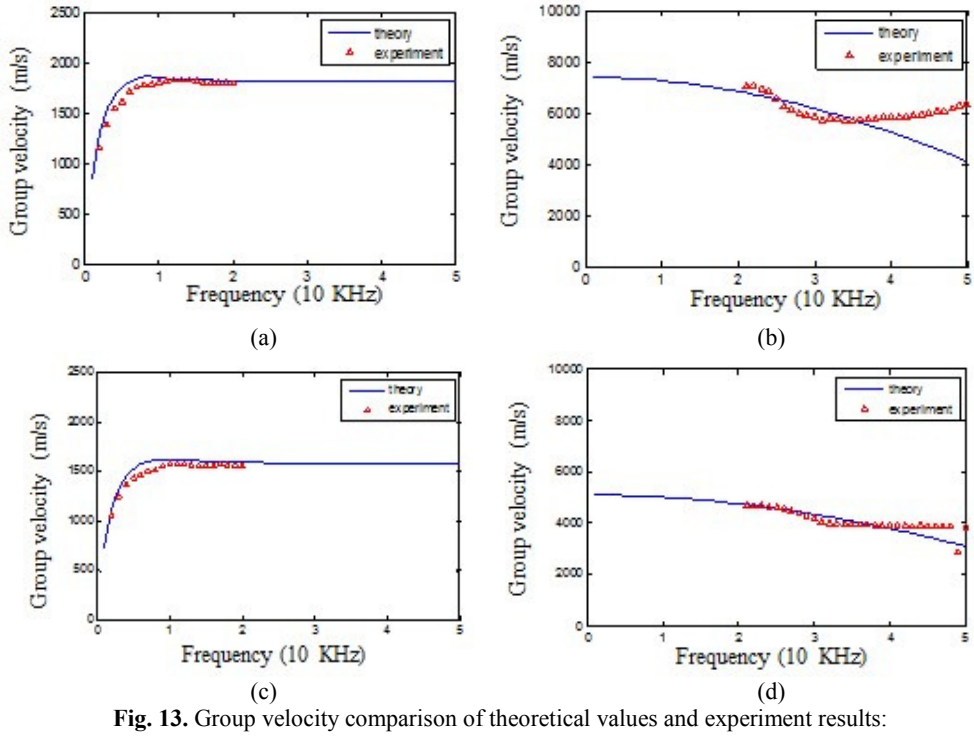

Fig. 13. Group velocity comparison of theoretical values and experiment results:
(a) A_0 mode in direction E_1, (b) S_0 mode in direction E_1,
(c) A_0 mode in direction E_2, (d) S_0 mode in direction E_2

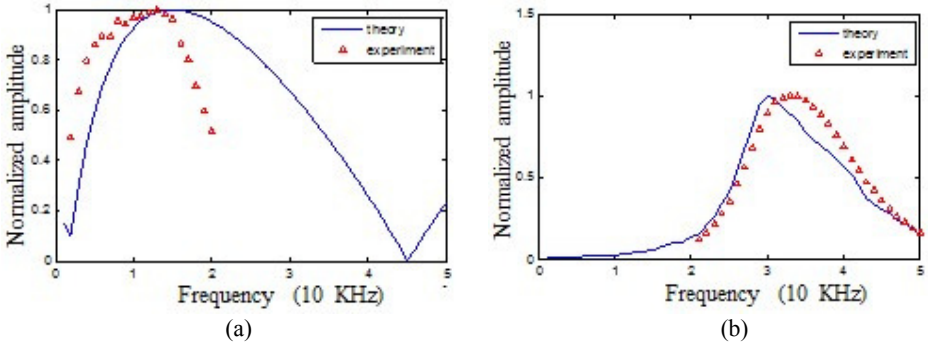

Fig. 14. Amplitude comparison of theoretical values and experiment results in direction E_1:
(a) A_0 mode, (b) S_0 mode

4.5 Waveform comparison

The response signals of Lamb wave is elongated because of the dispersion characteristic of stress wave propagating in plate structures. Since the analytical modeling assumes the waveform being the sinusoid function, several response sinusoid waveforms under different frequencies are added together to compare with the experimental wave form. The response signal in direction E_1 under the frequency 50 KHz is chosen. Three frequency spectrum amplitudes 125, 150 and 150 corresponding to the frequencies 40 KHz, 50 KHz and 60 KHz are extracted from Fig. 10(b). The three waveforms are modulated sine waves whose amplitudes are proportional to their respective spectrum amplitudes in Fig. 10(b) and response normalized amplitudes 0.46, 0.59 and 0.69 in Fig. 14(a). The three waveforms are delayed according to their respective theoretical group velocities, which are 1678 m/s, 1764 m/s and 1817 m/s and then added together.

For the S_0 mode waveform comparison, the central frequency 400 KHz is chosen. Three amplitudes 31.2, 25.6 and 25.6 corresponding to the frequencies 320 KHz, 400 KHz and 480 KHz are extracted from the corresponding frequency spectrum. The three waveforms are modulated sine waves whose amplitudes are proportional to their respective spectrum amplitudes and response normalized amplitudes 0.92, 0.56 and 0.21. They are all delayed according to their respective theoretical group velocities, which are 6025 m/s, 5259 m/s and 4357 m/s and then added together.

The added theoretical waveforms under the frequencies of 50 KHz and 400 KHz whose respective modes are A_0 mode and S_0 mode are shown in Fig. 15. The theoretical and experimental correlation is much better for the A_0 mode than the S_0 mode, which is consistent with the conclusion that the 2nd order Mindlin plate theory is suitable for analytical modeling under low frequencies.

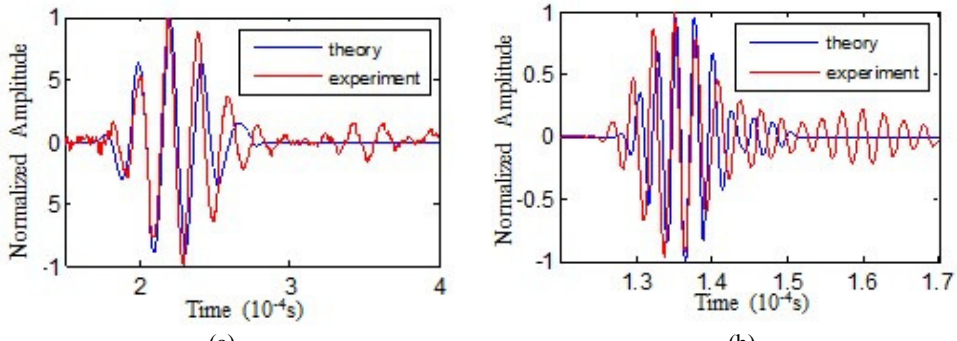

(a) (b)

Fig. 15. Wave form comparison of theoretical value and experiment results:
(a) A_0 mode under 50 KHz, (b) S_0 mode under 400 KHz

5. Conclusions

The Mindlin plate theory considers the influence of transverse shear deformation and moment of inertia on displacements. Thus it is more suitable for dynamic analysis of composite laminate with low transverse shear stiffness and large transverse shear deformation. Combining the adhesive coupling model of the piezoelectric actuator with the Mindlin plate theory, the dispersion curve of Lamb wave in any direction and mechanical parameters of any point in the composite are obtained, and thus the modeling of piezoelectric wafer excited Lamb wave propagating in composite laminate is realized. The experiment testifies that the analytical modeling effectively reflects the propagation characteristics of Lamb wave in composite

laminate regarding including the phase and group velocity dispersion characteristics, different phase and group velocities in different directions, and amplitudes variation with the central frequencies. The exact analytical modeling promotes the engineering application of SHM.

Acknowledgement

This work is supported by the Natural Science Foundation of China (Grant No. 50830201), the EU-FP7 SICA Programme (Grant No. FP7-PEOPLE-2010-IRSES-269202) and funded by the Priority Academic Program Development of Jiangsu Higher Education Institutions.

References

[1] **Chang F.-K., Markmiller J. F. C., Yang J., Kim Y.** Structural Health Monitoring System Health Management. John Wiley & Sons Ltd., 2011, p. 419 - 428.

[2] **Rose J. L.** Ultrasonic Waves in Solid Media. Cambridge, Cambridge University Press, 1999.

[3] **C. Boller** Next generation structural health monitoring and its integration into aircraft design. International Journal of Systems Science, Vol. 31, 2000, p. 1333 - 1349.

[4] **C. H. Wang, Fu-Kuo Chang** Scattering of plate waves by a cylindrical inhomogeneity. Journal of Sound and Vibration, Vol. 282, 2005, p. 429 - 451.

[5] **Neau G.** Lamb Waves in Anisotropic Viscoelastic Plates. Study of the Wave Fronts and Attenuation. Ph. D. Dissertation, L' University de Bordeaux, 2003.

[6] **Lei Wang, F. G. Yuan** Group velocity and characteristic wave curves of Lamb waves in composites: Modeling and experiments. Composites Science and Technology, Vol. 67, 2007, p. 1370 - 1384.

[7] **Lei Wang, F. G. Yuan** Damage identification in a composite plate using prestack reverse-time migration technique. Structural Health Monitoring, Vol. 4, 2005, p. 153 – 160.

[8] **Rose L. R. F., Wang C. H.** Mindlin plate theory for damage detection: Source solutions. Journal of the Acoustical Society of America, Vol. 116, Issue 1, 2004, p. 154 - 171.

[9] **Lowe M.** Matrix techniques for modeling ultrasonic waves in multilayered media. IEEE Transactions on Ultrasonics, Ferroelectrics and Frequency Control, 1995, Vol. 42, p. 525 - 542.

[10] **Lowe M. J. S., Cawley P.** The applicability of plate wave techniques for the inspection of adhesive and diffusion bonded joints. Journal of Nondestructive Evaluation, Springer, Netherlands, Vol. 13, 1994, p. 185 - 200.

[11] **Lei Wang** Elastic Wave Propagation in Composites and Least-Squares Damage Localization Technique. Master Thesis, North Carolina State University, 2003.

[12] **Horacio Sosa** Plane problems in piezoelectric media with defects. Solids Structures, Vol. 28, Issue 4, 1990, p. 491 - 505.

[13] **E. F. Crawley, De Luis** Use of piezoelectric actuators as elements of intelligent structures. AIAA Journal, Vol. 25, Issue 10, 1987, p. 1373 - 1385.

[14] **Zhang X., Yuan S., Hao T.** Lamb wave propagation modeling for structure health monitoring. Frontiers of Mechanical Engineering in China, Higher Education Press, Co-Published with Springer-Verlag GmbH, Vol. 4, 2009, p. 326 - 331.

[15] **Washizu K.** Variational Methods in Elasticity and Plasticity. Third Edition, Pergamon Press, Oxford, 1982.

[16] **Giurgiutiu V.** Structural Health Monitoring with Piezoelectric Wafer Active Sensors. Academic Press, 2008.